DOI: 10.1111/tgis.12800

RESEARCH ARTICLE

Transactions in GIS WILEY

Comparing the space-time patterns of high-risk areas in different waves of COVID-19 in Hong Kong

Zihan Kan[1] | Mei-Po Kwan[1,2,3] | Jianwei Huang[1] | Man Sing Wong[4] | Dong Liu[5,6,7]

[1]Institute of Space and Earth Information Science, The Chinese University of Hong Kong, Shatin, Hong Kong, China

[2]Department of Geography and Resource Management, The Chinese University of Hong Kong, Shatin, Hong Kong, China

[3]Department of Human Geography and Spatial Planning, Utrecht University, Utrecht, The Netherlands

[4]Department of Land Surveying and Geo-Informatics and Research Institute for Sustainable Urban Development, The Hong Kong Polytechnic University, Hung Hom, Hong Kong, China

[5]Department of Geography and Geographic Information Science, University of Illinois at Urbana-Champaign, Urbana, IL, USA

[6]Human Environments Analysis Laboratory, The University of Western Ontario, London, ON, Canada

[7]Department of Geography and Environment, The University of Western Ontario, London, ON, Canada

Correspondence
Mei-Po Kwan, Department of Geography and Resource Management and Institute of Space and Earth Information Science, The Chinese University of Hong Kong, Shatin, Hong Kong, China.
Email: mpk654@gmail.com

Abstract

This study compares the space-time patterns and characteristics of high-risk areas of COVID-19 transmission in Hong Kong between January 23 and April 14 (the first and second waves) and between July 6 and August 29 (the third wave). Using space-time scan statistics and the contact tracing data of individual confirmed cases, we detect the clusters of residences of, and places visited by, both imported and local cases. We also identify the built-environment and demographic characteristics of the high-risk areas during different waves of COVID-19. We find considerable differences in the space-time patterns and characteristics of high-risk residential areas between waves. However, venues and buildings visited by the confirmed cases in different waves have similar characteristics. The results can inform policymakers to target mitigation measures in high-risk areas and at vulnerable groups, and provide guidance to the public to avoid visiting and conducting activities at high-risk places.

This is an open access article under the terms of the Creative Commons Attribution-NonCommercial-NoDerivs License, which permits use and distribution in any medium, provided the original work is properly cited, the use is non-commercial and no modifications or adaptations are made.
© 2021 The Authors. *Transactions in GIS* published by John Wiley & Sons Ltd.

Funding information
RGC Postdoctoral Fellowship awarded by Research Grants Council of Hong Kong, Grant/Award Number: PDFS2021-4S08; Research Grants Council of Hong Kong, University Grants Committee, Grant/Award Number: 14605920, C4023-20GF and 15602619; Chinese University of Hong Kong, Grant/Award Number: 3133240; Hong Kong Polytechnic University, Grant/Award Number: 1-BBWD; University of Illinois at Urbana-Champaign

1 | INTRODUCTION

Since it was first identified in January 2020, Coronavirus Disease 2019 (COVID-19) has quickly spread around the world. Hong Kong has been affected by, and taken action in response to, the COVID-19 pandemic since January 2020. As one of the most densely populated cities in the world, Hong Kong has been hit by three waves of COVID-19 and is experiencing its fourth wave at the time of writing. As COVID-19 transmission is now widespread in Hong Kong, understanding the space-time patterns of the pandemic is critical for identifying at-risk groups and places and developing targeted interventions. This study aims to explain the presence of different waves of COVID-19 in Hong Kong by exploring the space-time patterns of high-risk areas during different waves of the pandemic and identifying the associated demographic and built-environment characteristics.

Timely analysis of case data during the COVID-19 pandemic can help understand the spatiotemporal spread of the pandemic and predict local outbreaks. Spatiotemporal statistics and analytic approaches are effective tools to highlight the spatiotemporal patterns of disease, which have been considered as an important task in the fields of geography, spatial epidemiology, and public health (Kirby, Delmelle, & Eberth, 2017; Robertson & Nelson, 2010). Among the various space-time analysis and statistical approaches, the space-time scan statistic is a popular and effective method for detecting significant clusters of disease occurrences and estimating the associated risk levels (Kulldorff, 2018). It has been widely applied in studies on identifying high-risk areas and periods of disease, examples of which include measles incidence in China (Tang et al., 2017), West Nile Virus infection in Italy (Mulatti et al., 2015), rash and respiratory diseases in the United States (Takahashi, Kulldorff, Tango, & Yih, 2008), and dengue fever in Panama (Whiteman, Desjardins, Eskildsen, & Loaiza, 2019). Recently, the space-time scan statistic has also been used to detect the clusters and model the trends of COVID-19 in the United States (Desjardins, Hohl, & Delmelle, 2020; Hohl, Delmelle, Desjardins, & Lan, 2020). The space-time scan statistic has two versions: prospective and retrospective scan statistics. The prospective space-time scan statistic is more suitable for case data that are updated daily. It can find emerging clusters by the end of the study period and is usually used in disease surveillance systems to monitor the early outbreak of diseases (Desjardins et al., 2020; Hohl et al., 2020; Kan, Kwan, Wong, Huang, & Liu, 2021; Kulldorff, 2001). The retrospective space-time scan can detect clusters occurring at any time over the study period and is used in applications where there are interests in both current and historical clusters (Prates, Kulldorff, & Assunção, 2014).

Much research has demonstrated that the occurrence and space-time development of diseases are significantly influenced by people's socioeconomic characteristics and local built-environment features (Huang et al., 2020; Kwok et al., 2021; Tiwari & Rushton, 2010). In the context of COVID-19, it was found by Mollalo, Vahedi, and Rivera (2020) that median household income, income inequality, percentage of Black female population, and percentage of nurse practitioners were associated with significant variations in COVID-19 incidence. Raifman and Raifman (2020) also reported that low-income people had a higher risk of infection with COVID-19 in the United States. In addition to socioeconomic characteristics, built-environment features can also affect people's health

outcomes. On the one hand, the design of spaces—such as ventilation systems and surface materials of buildings—may affect the spread of infectious disease, as certain diseases spread through the air and contaminated objects (Dietz et al., 2020). On the other hand, the built environment affects people's health by influencing their mobility, activity, and social interactions. Transportation systems, land use patterns, and urban design are the major domains in which the built environment exerts its effects on human health (Frank, Engelke, & Schmid, 2003). For instance, more green spaces may lead to better health through multiple pathways, including reducing people's exposure to air pollution, helping recovery from psychological stress, and encouraging people to increase their physical activity (Markevych et al., 2017). Other built-environment features—including singular land uses, poor-quality public open spaces, lower residential densities, inadequate health care, limited access to public transport, and social service infrastructure—are found to be associated with higher risks of health problems such as physical inactivity, poorer mental health, and obesity (Garfinkel-Castro, Kim, Hamidi, & Ewing, 2017; Koohsari, Badland, & Giles-Corti, 2013; Wang, Goggins, Zhang, Ren, & Lau, 2020). Past studies also show that human mobility patterns are related to built-environment features, especially land use (Gori, Nigro, & Petrelli, 2012; Soliman, Soltani, Yin, Padmanabhan, & Wang, 2017). As human movements may speed up virus transmission, mobility statistics are also used as indicators of the spread of COVID-19 in many studies (Gao, Rao, Kang, Liang, & Kruse, 2020; Kraemer et al., 2020).

The impact of the built environment on human health has been examined extensively in past studies. However, our knowledge of the relationship between built-environment features and the transmission of infectious disease is still limited, especially in the local context of COVID-19. As the pandemic is ongoing worldwide, many countries and cities have experienced several waves of COVID-19, strong interventions such as lockdowns, and gradual relaxation of these interventions. Examining the high-risk areas of transmission and their characteristics in different waves of COVID-19 is crucial for understanding the underlying mechanisms of the patterns of high-risk locations, predicting the dynamic patterns of COVID-19, and developing interventions that target the vulnerable locations and groups in a timely manner. This study compares the space-time patterns of high-risk areas of COVID-19 during the first and second waves and the third wave in Hong Kong, using contact tracing data of individual confirmed cases. The

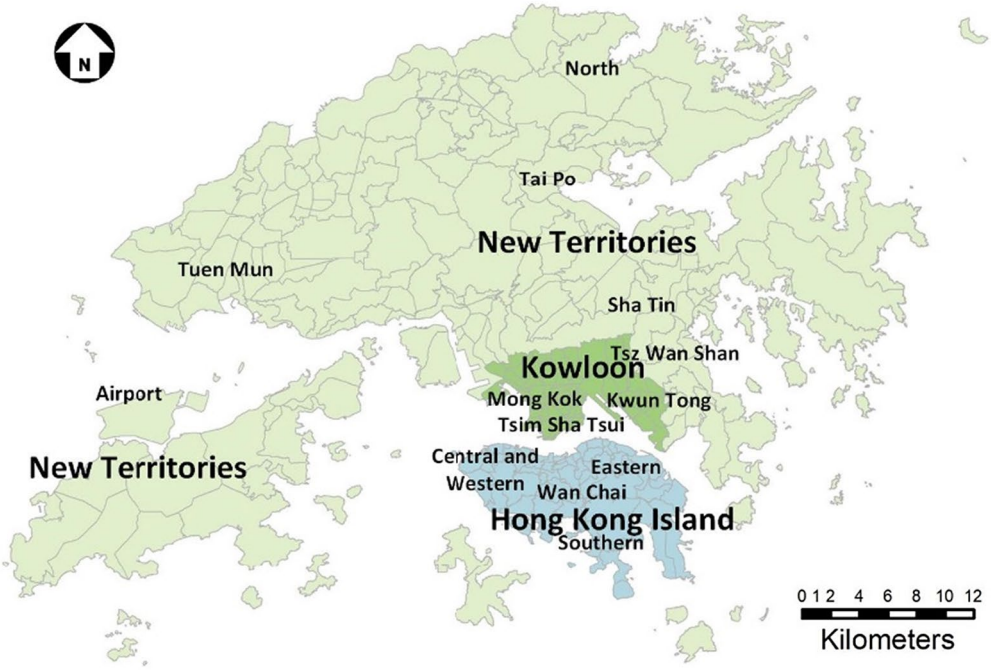

FIGURE 1 The study area: Hong Kong

demographic and built-environment characteristics of the high-risk areas in different waves of COVID-19 are further analyzed, which generates meaningful insights into the COVID-19 landscape in Hong Kong.

2 | DATA AND METHODOLOGY

2.1 | Study area and data

Hong Kong is the study area of this research (Figure 1). It is one of the most densely populated cities in the world. As of 2019, there were 7.4 million people living in its 1,104 km^2 area, which consists of Hong Kong Island, the Kowloon Peninsula, and the New Territories with 18 districts. The study unit of this research is the large street block group (LSBG), which is a group of street blocks with similar demographic status. There are 1,622 LSBGs with 1,000 or more residents according to the 2016 Hong Kong Census. The population in each LSBG ranges from 1,001 to 45,100, with a mean population of 4,522.43 and a median population of 2,379.

The data of daily individual confirmed COVID-19 cases used in this study were acquired from the Hong Kong Centre for Health Protection. We collected individual case data during January 23–April 14 (the first and second waves) and during July 7–August 29 (the third wave), 2020 (Figure 2). There were 1,013 confirmed cases in the first and second waves and 3,501 cases in the third wave. The record of each confirmed case includes age, gender, type (there are six types of cases: imported cases, local cases, cases linked with imported cases, cases linked with local cases, cases linked with possibly local cases, possibly local cases), and the residential buildings and buildings or venues visited by the confirmed cases in the past 14 days of confirmation. The temporal distribution of different types of confirmed cases is shown in Figure 2, in which the majority of cases in the first and second waves were imported cases, and the majority of cases in the third wave were local cases.

We categorized the six types of cases into two general groups: local cases (including local cases, possibly local cases, cases linked with local cases, cases linked with possibly local cases) and imported cases (including imported cases and cases linked with imported cases). Based on the two groups of cases, we then categorized the case-related locations into four types: LR = residences of local cases; IR = residences of imported cases; LV = locations visited by local cases; and IV = locations visited by imported cases. LR and IR indicate the incidence of COVID-19 by the residential location of the confirmed cases, while LV and IV indicate the spatial interactions between the confirmed cases and locations (through the places they visited), which might be potential sources of COVID-19 transmission.

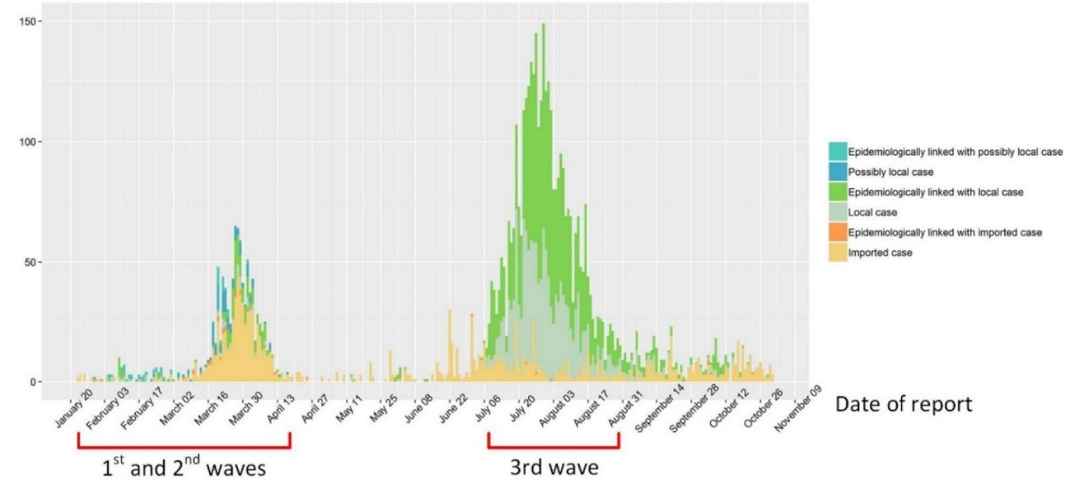

FIGURE 2 COVID-19 cases in Hong Kong by dates of confirmation

Demographic data used in this study are population and median household income in 2016. The data were obtained from the Hong Kong Census and Statistics Department and aggregated at the level of LSBG. LSBG-level built-environment features, including building density, average building height, nodal accessibility, sky view, green spaces, and land use, are derived from a variety of geospatial data sources. Building density and average building height are calculated from a 3D building dataset provided by the Hong Kong Planning Department. The sky view factor is defined as the ratio of the amount of sky visible from a location on the ground to the amount of sky that is potentially available. The sky view dataset is a 10 × 10 m raster calculated from multiple geospatial datasets, including building GIS data, land cover data, and airborne LiDAR data in a previous study (Yang, Wong, Menenti, & Nichol, 2015). The green spaces are represented by the normalized difference vegetation index (NDVI), calculated from SPOT-7 satellite images (in 2017) with a 1.5-m resolution. Nodal accessibility represents how well a transport node (e.g., a subway station or a bus stop) is connected with other nodes in a transport network. It is calculated from the connectivity matrix of the transport nodes in each LSBG. The transport network dataset is obtained from the Hong Kong Transport Department. Since over 80% of trips in Hong Kong are made by public transport, we only consider the public transport networks, including the Mass Transit Railway (MTR), bus, and ferry.

Data of land use are acquired from a 10 × 10 m raster dataset of land use from the Hong Kong Planning Department. There are 27 types of land use in the dataset, and this study includes four of them: private residential land density, public residential land density, commercial land density, and open spaces and recreational land density. The density of each of these land use types in an LSBG is calculated by dividing the area of each type of land use in an LSBG by the area of the LSBG. In addition, a land use mix index (LUMI) in each LSBG is calculated based on the notion of entropy, as Equation (1) shows:

$$\mathrm{LUMI} = -\sum_{i=1}^{N} \frac{L_i * \ln L_i}{N} \tag{1}$$

where L_i represents the proportion of the ith type of land use, and N is the total number of land use types in the LSBG.

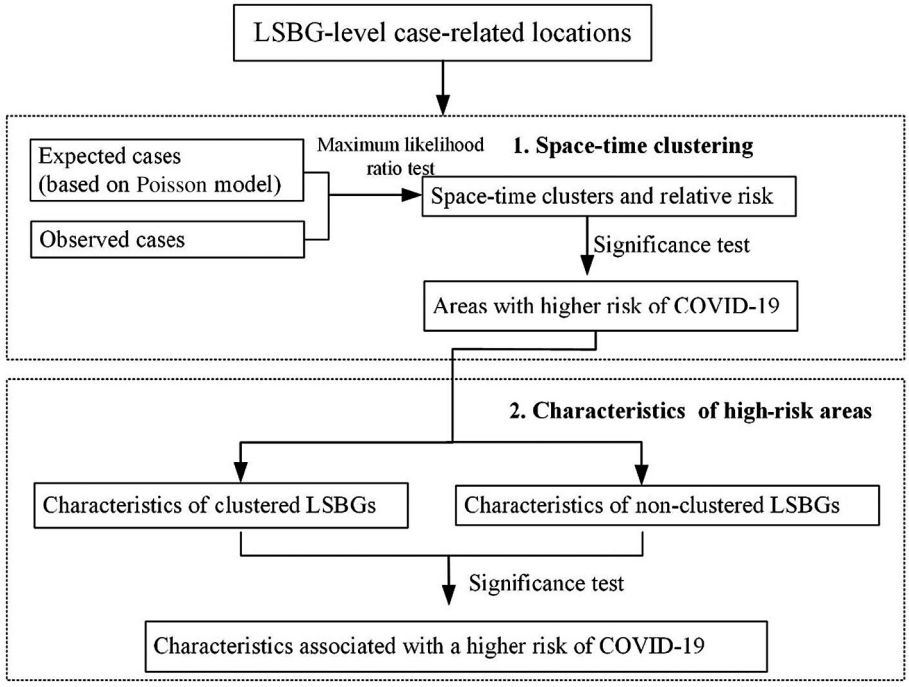

FIGURE 3 Conceptual model of this study

2.2 | Methodology

Figure 3 shows the conceptual model of this study. The study first identifies the space-time clusters of the case-related locations. A discrete Poisson model is used to estimate the expected number of cases in each LSBG within various spatial and temporal windows. By comparing the observed number of cases with the expected number of cases in each spatial-temporal window, space-time clusters are detected based on a maximum likelihood ratio test and the relative risks of clusters and LSBGs are calculated for the clusters and LSBGs within clusters. A significance test is then conducted for the identified clusters, and areas with significantly higher risk of COVID-19 transmission are then detected. Based on the results of space-time clusters, this study further analyzes the demographic and built-environment characteristics associated with areas with higher risk levels by comparing the characteristics associated with the LSBGs in the detected clusters with those associated with the LSBGs outside the clusters. A significance test is also conducted to determine the significant characteristics that differentiate between the clustered LSBGs and non-clustered LSBGs. As a result, characteristics associated with higher risk in different waves of COVID-19 in Hong Kong are examined.

2.2.1 | Identify space-time clusters with high COVID-19 transmission risk

This study analyzes the space-time patterns of COVID-19 in Hong Kong by detecting significant space-time clusters of the four types of case-related locations: LR, IR, LV, and IV. Given the four types of locations aggregated at the LSBG level, space-time scan statistics implemented in the SaTScan™ software package (Kulldorff, 2018) are used in this study for cluster detection. We use the discrete Poisson model as the baseline model for the space-time scan statistics. For residential locations (IR and LR), the null hypothesis is that the expected number of COVID-19 cases follows a discrete Poisson distribution based on the population in each LSBG. The alternative hypothesis states that the number of observed COVID-19 cases exceeds the number of expected cases derived from the null model (Desjardins et al., 2020; Hohl et al., 2020). For visited locations (IV and LV), the null hypothesis is that the expected number of visits follows a discrete Poisson distribution based on the number of buildings or venues in each LSBG. With the scan statistics, a space-time cluster is detected when the observed number of cases in a time period exceeds the expected number of cases in the same time period based on the maximum likelihood ratio test. Monte Carlo simulation is used to test the statistical significance of the detected clusters. Since an LSBG is more likely to be detected as a component of a cluster if the number of observed cases in the LSBG is significantly higher than the number of expected cases in the LSBG, the population in an LSBG will affect the clustering as it determines the expected number of cases in each LSBG, while the geographic size of an LSBG only affects the size of the cluster.

Based on the detected space-time clusters, the values of relative risk are calculated for the clusters and LSBGs within the clusters. The relative risk of a detected cluster is calculated as Equation (2) shows:

$$\mathrm{RR} = \frac{n/e}{(N-n)/(N-e)} \tag{2}$$

where RR is the relative risk of a cluster; n and N are the total numbers of confirmed cases in the cluster and the entire study area; e is the number of expected cases in the cluster. Equation (2) depicts that the relative risk of a cluster is its estimated risk divided by that outside it. A relative risk value higher than 1 means that the cluster has a higher risk of disease exposure compared with locations outside the cluster, and the higher the relative risk value is, the higher the possibility of disease exposure. In the same way, relative risk can also be calculated for an LSBG by dividing the estimated risk within the LSBG by that outside the LSBG. So, an LSBG is likely to be detected as a component of a cluster if the number of observed cases in the LSBG is significantly higher than the number of expected cases in the

LSBG. Therefore, the population in an LSBG will affect the clustering as it determines the expected number of cases in each LSBG, while the geographic size of an LSBG only affects the size of the cluster.

In this study, we use retrospective SatScan instead of prospective SatScan because we intend to detect clusters that emerged at any time during the study period. Moreover, our study period covers the complete first, second and third waves of COVID-19 in Hong Kong. The number of confirmed cases was stable and there were few emerging clusters by the end of each wave (Figure 2). Therefore, retrospective SatScan is more suitable for our dataset.

2.2.2 | Analyze the characteristics of areas with higher risks of COVID-19 transmission

This study analyzes the demographic and built-environment characteristics associated with the detected clusters by comparing the characteristics associated with LSBGs in the detected clusters with those associated with LSBGs outside the clusters.

Based on the four categories of detected clusters (i.e., LR, IR, LV, IV), we identify LSBGs in and outside each type of cluster, resulting in two groups of LSBGs: clustered LSBGs and non-clustered LSBGs. Then we compare the features associated with the two groups of LSBGs. The distributions of the features in the two LSBG groups are visualized in a series of boxplots. We further explore whether the differences between the features in the two groups are statistically significant. In order to test the statistical significance, we first check the distribution of each feature in the two groups. The results show that none of the features follows a normal distribution. Due to the non-normal distribution of the data, we use the non-parametric Mann–Whitney *U* test to determine the significance of the difference in each feature between the clustered LSBGs and non-clustered LSBGs. If the difference is significant, we have strong evidence that the feature is associated with a higher risk of occurrence and transmission of COVID-19.

3 | RESULTS

3.1 | Space-time clusters of COVID-19 cases

In order to determine the optimal spatial and temporal windows for the space-time statistic, we tested six different combinations of spatial and temporal windows on the residential location data based on all confirmed cases (please note that the data we tested were not divided into the residential locations of local cases and imported cases). We selected 1% population at risk, 3% population at risk, and 5% population at risk as the spatial windows, and 30% of the study period and 50% of the study period as the temporal windows. We did not select larger spatial and temporal windows in order to avoid detecting extremely large clusters. We found that the detected clusters are generally stably distributed under different spatial and temporal windows, and temporal windows do not have significant impact on the distribution and number of detected clusters. When using a spatial window of 1% of the population and 30% and 50% of the study period as the temporal windows, many of the detected clusters contain only one LSBG and are considered too small. With the spatial window of 3% of the population and temporal windows of 30% and 50% of the study period, some smaller clusters have merged into larger clusters. When using a spatial window of 5% of the population and 30% and 50% of the study period as the temporal windows, some areas in Kowloon and Hong Kong Island that are geographically separated by Victoria Harbor are detected as one cluster. We therefore consider the spatial window of 5% of the population is too large for the area of Hong Kong. Because the temporal window is the largest time span for detecting clusters, we select 50% instead of 30% of the study period in order to detect clusters with the maximum likelihood in a larger time span. Therefore, we chose 3% of the population and 50% of the study period as the spatial and temporal windows. In addition, each detected cluster must have at least two cases and a minimum duration of 2 days to avoid extremely small clusters.

TABLE 1 Space-time clusters of local COVID-19 cases (LR) in the first and second waves of COVID-19 in Hong Kong

Cluster	Duration	Observed	Expected	Relative risk	*p*-Value	No. LSBGs
1	March 22–April 4	34	0.67	55.48	0	39
2	March 18–30	22	0.39	59.89	0	19
3	March 20–April 2	13	0.20	66.16	.000	9
4	April 1–9	6	0.01	450.37	.000	1
5	March 19–April 1	12	0.63	19.67	.000	32
6	March 21–April 1	10	0.38	26.63	.000	2
7	March 27–30	5	0.03	163.18	.000	3
8	March 26–29	6	0.12	50.79	.000	10
9	March 18–23	6	0.13	47.01	.000	7
10	March 27–30	6	0.18	34.01	.016	20
11	March 17–April 3	5	0.11	44.64	.041	5

TABLE 2 Space-time clusters of local COVID-19 cases (LR) in the third wave of COVID-19 in Hong Kong

Cluster	Duration	Observed	Expected	Relative risk	*p*-Value	No. LSBGs
1	July 8–August 1	211	14.98	14.98	0	9
2	July 24–31	36	0.07	486.63	0	1
3	July 30–August 5	41	4.33	9.56	0	17
4	July 31–August 18	49	10.48	4.73	.00	18
5	July 27–August 18	56	13.67	4.15	.00	24
6	July 22–August 9	48	11.27	4.30	.00	38
7	July 23–25	5	0.02	196.17	.00	1
8	August 6–7	5	0.04	105.24	.00	1
9	August 17–20	5	0.05	101.89	.00	1
10	July 25–August 2	22	4.68	4.72	.00	13

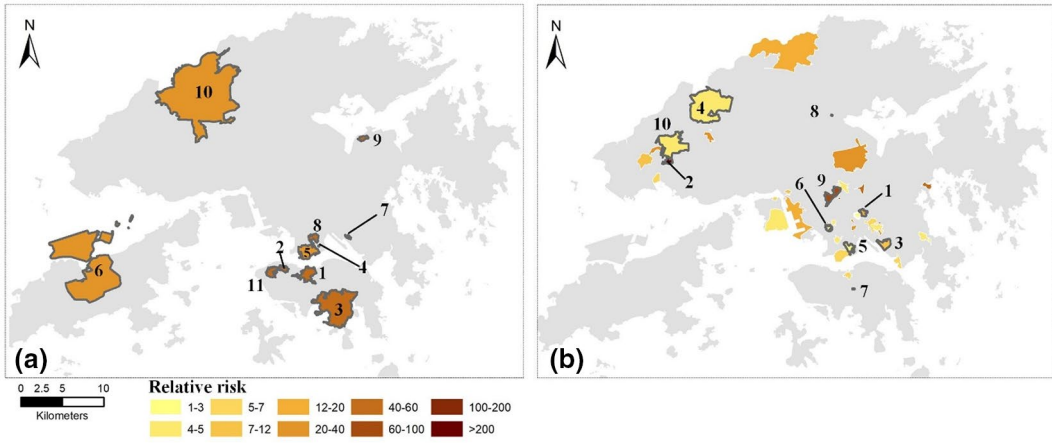

FIGURE 4 Distribution of the space-time clusters of the residential buildings of local cases (LR) in: (a) the first and second waves; and (b) the third wave of COVID-19 in Hong Kong

3.1.1 | Space-time clusters of the residences of local cases

Tables 1 and 2 and Figure 4a,b show the characteristics and spatial distribution of the space-time clusters of the residences of local cases (LR clusters) in the first and second waves and the third wave of COVID-19. There were 11 clusters in the first and second waves in Figure 4a and Table 1, and 41 clusters in the third wave in Figure 4b, from which we only report 10 clusters with higher relative risks and more at-risk population in Table 2.

Figure 4a shows that most of the LR clusters in the first and second waves were located on Hong Kong Island and in Kowloon. A total of 72 LSBGs in Clusters 1–3 and 11 were located on Hong Kong Island, with relative risk values ranging from 44.64 to 66.16. Clusters 4–5 and 7–8, including 46 LSBGs, were located in Kowloon, with relative risk values from 19.67 to 450.37. The cluster with the highest relative risk (i.e., 450.37) occurred between April 1 and April 9 and was located in a neighborhood in Kowloon City District. The cases in the cluster were family members and friends infected in a group outbreak caused by band performances in bars. Clusters 6, 9, and 10, with 29 LSBGs, were located in the New Territories, with relative risk values from 26.63 to 47.01. Among them, Cluster 6 was located near the airport. There are many residential buildings for the staff of the Hong Kong International Airport and airlines, who are high-risk groups for COVID-19 infection.

In comparison, in the third wave of COVID-19 as shown in Table 2 and Figure 4b, most of the clusters were located in Kowloon and the New Territories. In Figure 4b, only two clusters with a total of 19 LSBGs were located on Hong Kong Island. In Table 2, Clusters 1, 3, 5, and 6, with 88 LSBGs, were located in Kowloon, with relative risk values from 4.15 to 14.98. Cluster 1 occurred in Tsz Wan Shan, where a neighborhood outbreak occurred in the early stage of the third wave of COVID-19. There were 38 LSBGs in Cluster 6, and these LSBGs were located in the lower-income neighborhoods in Sham Shui Po District. Clusters 2, 4, 8–9, and 10, with 34 LSBGs, were located in the New Territories, with relative risk values from 4.72 to 486.63. Cluster 2 was an outbreak in a nursing home for the elderly in Tuen Mun District.

3.1.2 | Space-time clusters of locations visited by local cases

Tables 3 and 4 and Figure 5a,b show the characteristics and distribution of the space-time clusters of buildings or venues visited by local COVID-19 cases (LV clusters) in the first and second waves and the third wave of COVID-19. There are 19 clusters in the first and second waves in Figure 5a and 29 clusters in the third wave in

TABLE 3 Space-time clusters of places visited by local cases (LV) in the first and second waves of COVID-19 in Hong Kong

Cluster	Duration	Observed	Expected	Relative risk	*p*-Value	No. LSBGs
1	March 18–April 8	162	1.56	140.13	.00	32
2	March 25–April 2	70	0.16	500.16	.00	9
3	February 23–April 3	50	3.00	18.07	.00	92
4	March 18–31	25	1.02	25.39	.00	121
5	March 17–April 2	10	0.08	124.17	.00	1
6	March 20–29	14	0.73	19.68	.00	22
7	March 18–31	13	0.75	17.59	.00	50
8	March 18–April 4	14	1.28	11.21	.00	45
9	March 29–April 2	5	0.03	166.88	.00	1
10	April 1–3	5	0.06	88.92	.00	12

TABLE 4 Space-time clusters of buildings/venues visited by local cases (LV) in the third wave of COVID-19 in Hong Kong

Cluster	Duration	Observed	Expected	Relative risk	*p*-Value	No. LSBGs
1	July 10–23	173	0.01	>500	.00	1
2	July 7–27	182	7.82	25.31	.00	43
3	July 12–29	137	7.02	20.76	.00	129
4	July 9–August 4	109	9.69	11.78	.00	48
5	July 19–August 13	93	10.21	9.47	.00	49
6	July 15–August 10	59	7.43	8.13	.00	20
7	July 20–23	17	0.24	71.39	.00	11
8	August 23–29	7	0.06	115.20	.00	1
9	July 21–22	5	0.02	207.17	.00	1
10	August 6–9	5	0.05	105.70	.00	1

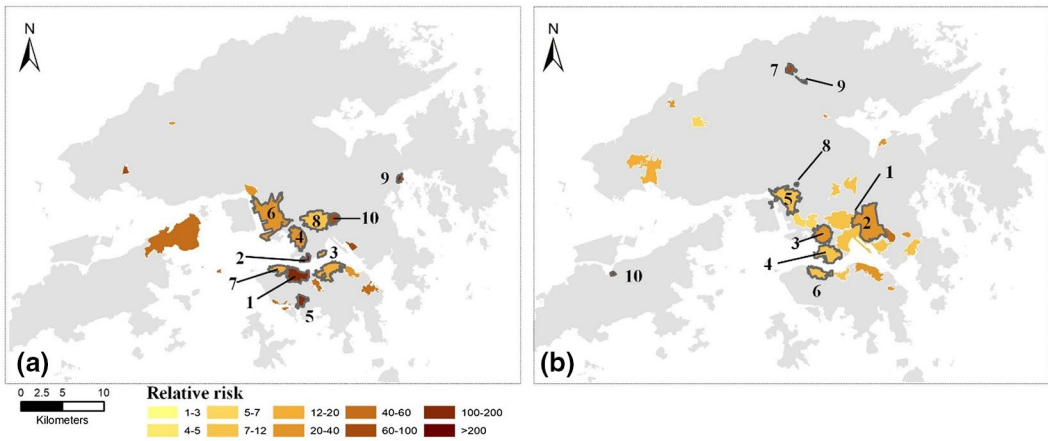

FIGURE 5 Space-time clusters of places visited by local cases in: (a) the first and second waves; and (b) the third wave of COVID-19 in Hong Kong

Figure 5b. We also only report 10 clusters with higher relative risks and more at-risk population for the first and second waves and the third wave in Tables 3 and 4.

In Table 3 and Figure 5a, the LV clusters were mainly distributed in Kowloon and on Hong Kong Island, and only a small number of clusters occurred in the New Territories. Clusters 1, 3, 5, and 7, with a total of 175 LSBGs and 215 visits, were located on Hong Kong Island. Cluster 1, with a relative risk of 140.13 and 162 visits during March 18–April 8, was located near Central on Hong Kong Island, which has a high density of dining and entertainment venues. Multiple group outbreaks occurred in this cluster (e.g., in nightclubs and gyms). Clusters 2, 4, 8, and 10, with a total of 187 LSBGs and 114 visits, were located in Kowloon. Cluster 2 had the highest relative risk of around 500. It was located in Tsim Sha Tsui and received 70 visits during the week between March 25 and April 2, where a group outbreak occurred in a *karaoke* bar. Two clusters were located in the New Territories (i.e., Clusters 6 and 9). Cluster 9 had a relative risk of 166.88, receiving five visits between March 29 and April 2. It was in a country park in Sai Kung where many people go hiking.

In the third wave of COVID-19, in Table 4 and Figure 5b, more clusters were located in Kowloon and the New Territories than on Hong Kong Island. Cluster 6, with 59 visits and a relative risk of 8.13 from July 15 to August 10, was located near Central on Hong Kong Island. The locations visited by confirmed cases include a variety of venues such as restaurants, shopping malls, and other commercial buildings. Clusters 1–4 were located in Kowloon, with a total of 221 LSBGs and 601 visits. Cluster 1 had a very high relative risk of over 500, with 162 visits. It was located in Tsz Wan Shan, a residential area where a serious outbreak of local cases occurred in the third wave of COVID-19. The confirmed cases visited various venues, including markets and some restaurants frequently visited by taxi drivers, which became potential sources of further transmission. Clusters 5 and 7–10 were located in the New Territories, with 52 LSBGs and 127 visits. High-risk areas of group outbreaks included Kwai Chung container terminals (Cluster 8), North District (Clusters 7 and 9), and Island District (Cluster 10).

3.1.3 | Space-time clusters of the residences of and locations visited by imported cases

Table 5 and Figure 6a show the space-time clusters of residential buildings of imported cases (IR) in the first and second waves. We report 10 clusters with a higher relative risk and at-risk population out of 17 IR clusters. Figure 6a shows that most of the clusters were concentrated on Hong Kong Island and the New Territories, and only a few of the clusters were located in Kowloon. Most of the significant clusters in Table 4 occurred in later March and early April, during which a large number of overseas residents returned to Hong Kong due to the increasingly severe COVID-19 outbreak in some countries abroad (e.g., the UK and USA). Clusters 1, 2, 6, and 7 were located on Hong Kong Island, with 103 cases in 108 LSBGs and relative risk values from 13.52 to 34.25. Those clusters were mainly wealthy residential neighborhoods in Wan Chai District, Eastern District, and Southern District, as well as affluent neighborhoods at Mid-Levels. Clusters 3 and 9 were located in Kowloon, with 29 cases and 37 LSBGs. Clusters 4, 5, 8, and 10 were located in the New Territories, with 45 cases in 45 LSBGs. Among these clusters, Cluster 5 was located in Sai Kung, which is a wealthy area in East New Territories.

There are no significant IR clusters in the third wave of COVID-19 in Hong Kong, because few cases were imported from other countries, as shown in Figure 2. Moreover, during the third wave, most individuals were required to test for COVID-19 before entering Hong Kong. The confirmed cases were immediately sent to hospitals for medical attention and thus no residential locations were reported for these cases.

Tables 6 and 7 and Figure 6b,c show the space-time clusters of the buildings/venues visited by imported cases in the first and second waves and the third wave of COVID-19 in Hong Kong. The Hong Kong Government

TABLE 5 Space-time clusters of imported COVID-19 cases (IR) in the first and second waves of COVID-19 in Hong Kong

Cluster	Duration	Observed	Expected	Relative risk	*p*-Value	No. LSBGs
1	March 18–April 13	48	1.55	34.25	.00	30
2	March 18–April 6	23	1.00	24.10	.00	30
3	March 16–April 11	15	0.45	34.04	.00	11
4	March 16–April 11	14	0.36	40.05	.00	7
5	March 14–April 8	18	1.23	15.19	.00	30
6	March 20–April 8	15	0.79	19.58	.00	21
7	March 13–April 4	17	1.30	13.52	.00	27
8	March 22–April 10	10	0.28	36.60	.00	4
9	March 20–April 10	14	0.98	14.71	.00	26
10	March 23–28	3	0.04	75	.00	4

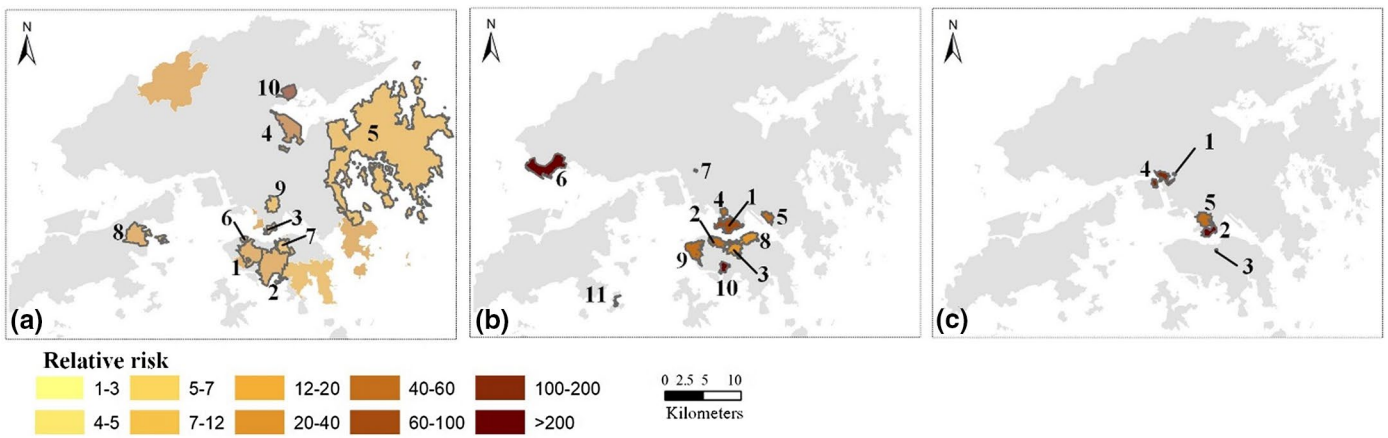

FIGURE 6 Distribution of the space-time clusters of the residential buildings of imported cases (IR) and buildings and venues visited by imported cases (IV): (a) IR clusters in the first and second waves; (b) IV clusters in the first and second waves; and (c) IV clusters in the third wave

TABLE 6 Space-time clusters of buildings/venues visited by imported COVID-19 cases (IV) in the first and second waves of COVID-19 in Hong Kong

Cluster	Duration	Observed	Expected	Relative risk	*p*-Value	No. LSBGs
1	March 14–April 9	55	0.96	70.03	.00	55
2	March 4–April 10	38	1.01	42.87	.00	23
3	March 4–April 9	31	1.03	33.57	.00	41
4	March 11–April 7	13	0.30	44.78	.00	26
5	March 11–April 1	12	0.26	48.26	.00	20
6	March 9–10	6	0.02	263.07	.00	4
7	March 25–April 9	5	0.01	>500	.00	1
8	March 22–April 9	11	0.43	26.67	.00	62
9	March 4–12	8	0.15	54.30	.00	10
10	March 22–30	5	0.02	245.04	.00	1
11	March 6–11	5	0.08	66.14	.01	1

TABLE 7 Space-time clusters of buildings/venues visited by imported COVID-19 cases (IV) in the third waves of COVID-19 in Hong Kong

Cluster	Duration	Observed	Expected	Relative risk	*p*-Value	No. LSBGs
1	July 7–31	12	0.0056	>500	.00	1
2	July 11–21	10	0.0496	234.96	.00	11
3	July 9–22	5	0.0055	>500	.00	1
4	July 8–13	5	0.0316	170.16	.00	26
5	August 15–24	6	0.1202	54.51	.00	81

required that individuals returning to Hong Kong from March 19 must go through a 14-day mandatory quarantine. Some of these visited buildings (e.g., bars) were visited by returnees before March 19, while some other buildings were hotels used by some of the returnees for self-quarantine. There was a total of 11 IV clusters in Table 6, in which Clusters 2, 3, 8, 9, and 10, with 137 LSBGs and 93 visits, were located on Hong Kong Island in areas with high commercial densities. Clusters 1, 4, and 5 were located in Kowloon, with 101 LSBGs and 80 visits. Characteristics of these locations are similar to those on Hong Kong Island. Clusters 6, 7, and 11, with 16 visits and 5 LSBGs, were located in the New Territories. Compared with the clusters in Kowloon and Hong Kong Island, the clusters in the New Territories received fewer visits and contained fewer LSBGs, but have higher relative risks. The higher relative risks were contributed by lower population and building densities in the locations in the New Territories, which decreased the expected number of visits by confirmed cases.

As shown in Table 7 and Figure 6c, there were only four IV clusters in the third wave of COVID-19. Clusters 1 and 3 were located in the New Territories and on Hong Kong Island, and all of the visited buildings in these clusters were hotels for quarantine. Clusters 2 and 5 were located in Kowloon, receiving 16 visits and with 92 LSBGs. The locations in the clusters were mainly hotels, while a few commercial buildings and an art museum were visited by an imported case who got a positive test result for COVID-19 after a 14-day quarantine in a hotel. Cluster 4 was located in the New Territories, with 26 LSBGs and 5 visits. The buildings in Cluster 4 include hotels and a restaurant visited by a cargo plane pilot who was exempted by the 14-day quarantine rule.

In summary, different space-time patterns of the residences of, and buildings and venues visited by, confirmed cases between the first and second waves and the third wave are observed. The results of the space-time clustering show that the clusters in the first and second waves mainly occurred on Hong Kong Island and in Kowloon.

The confirmed cases were mainly imported cases who studied or worked abroad and returned to Hong Kong as the COVID-19 situation overseas deteriorated. Many of these imported cases lived in relatively affluent areas on Hong Kong Island, and there were few outbreaks in local neighborhoods. In the third wave, however, there were many outbreaks in local residential neighborhoods. Clusters in the New Territories increased, while clusters on Hong Kong Island decreased compared with the first and second waves. The outbreaks occurred in lower-income neighborhoods and among vulnerable groups, such as the elderly and staff in Tuen Mun nursing homes. In terms of location visited, the major venues visited by confirmed cases in the first and second waves were mainly entertainment and commercial venues, such as bars and gyms, while the third wave involved a wider range of places, including workplaces, restaurants, and markets.

3.2 | Associated demographic and built-environment characteristics of areas with higher transmission risks of COVID-19

Based on the space-time patterns of the clusters in the first and second waves and the third wave of COVID-19, we now examine the demographic and built-environment characteristics associated with different types of clustered

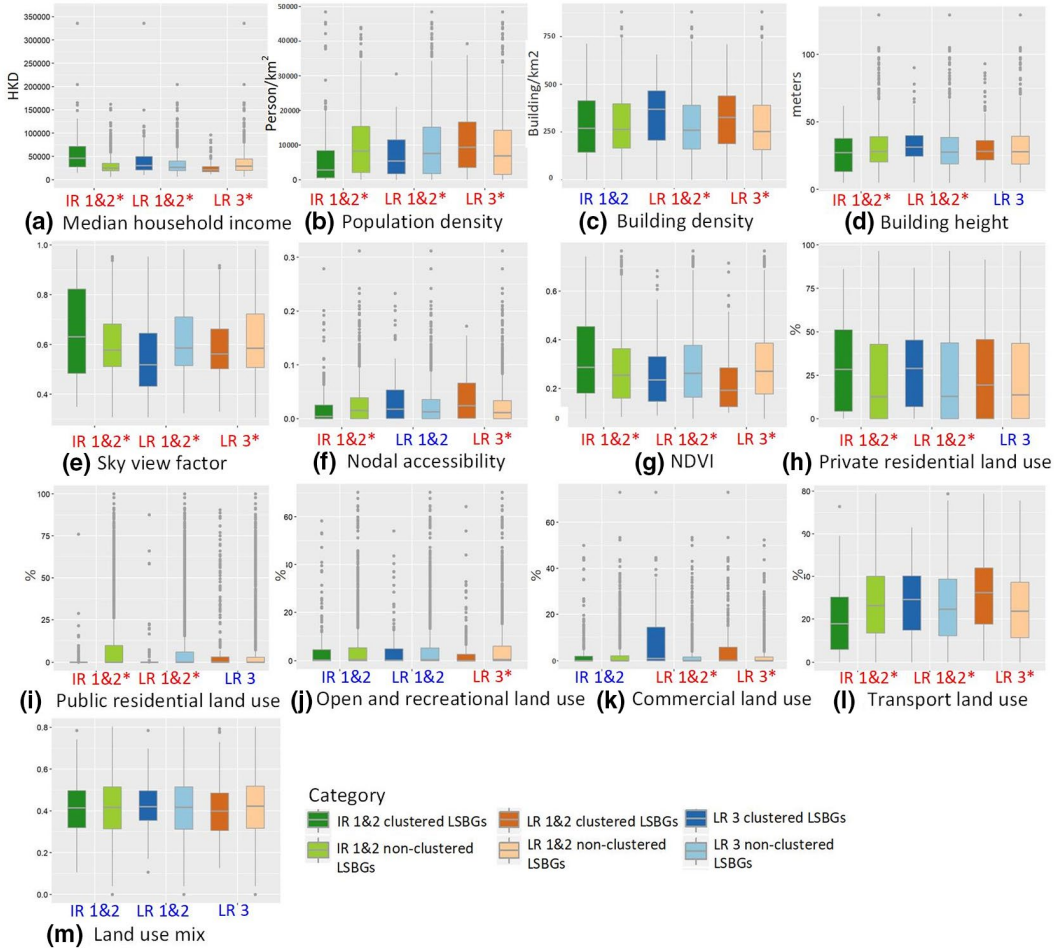

FIGURE 7 Features distribution of clustered LSBGs and non-clustered LSBGs for residences of imported cases and local cases in the first and second waves, and of local cases in the third wave of COVID-19 in Hong Kong

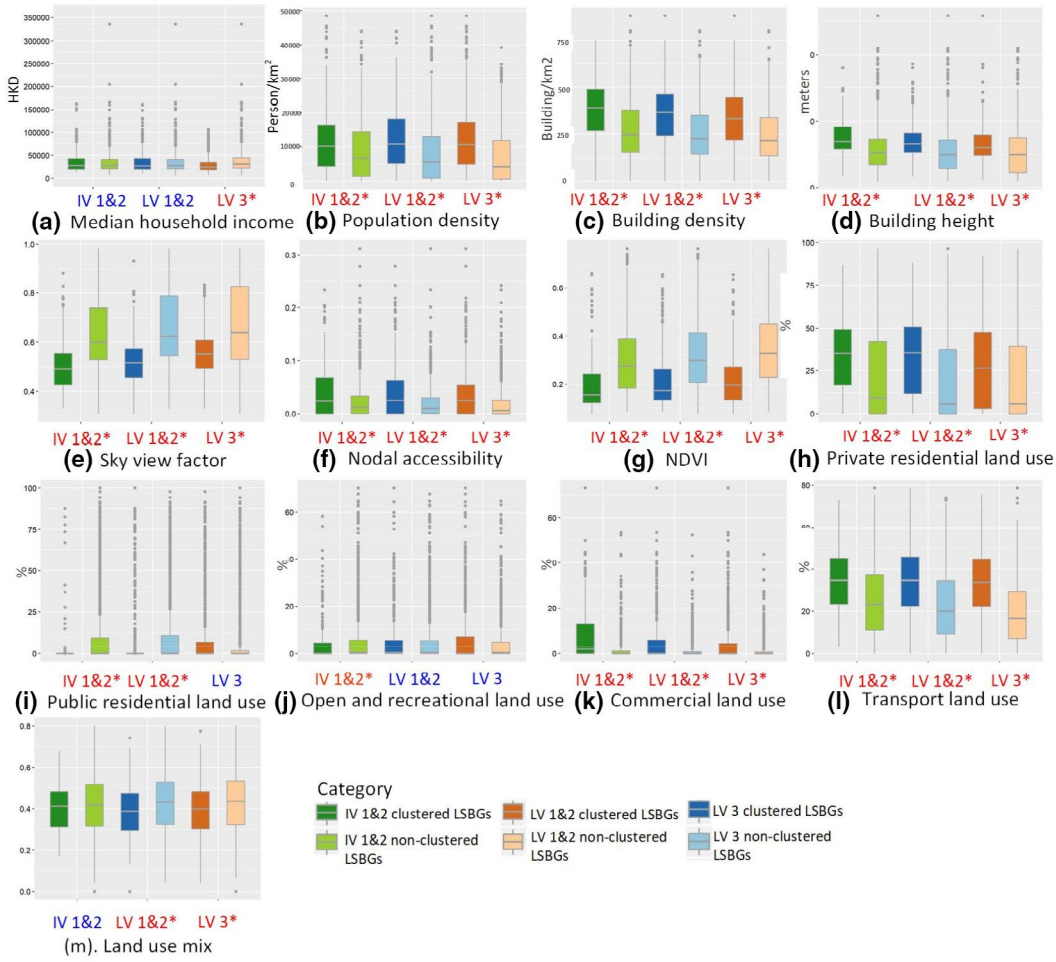

FIGURE 8 Features distribution of clustered LSBGs and non-clustered LSBGs for residences of imported cases and local cases in the first and second waves, and of local cases in the third wave of COVID-19 in Hong Kong

LSBGs (i.e., LR, LV, IR, and IV). Demographic features in this analysis are the median household income and population density in each LSBG. Eleven built-environment features are considered in this study: building density, building height, the sky view factor, nodal accessibility, green spaces (derived from the NDVI), private residential land density, public residential land density, open spaces and recreation land density, commercial land density, and the LUMI.

Figures 7 and 8 are the comparison results of different features between the clustered LSBGs and the non-clustered LSBGs of the residences of, and venues or buildings visited by, confirmed cases. The boxplots show the distribution of the features of the clustered LSBGs and non-clustered LSBGs. In Figure 7, "IR 1&2," "LR 1&2," and "LR 3" represent "residences of imported cases in the first and second waves," "residences of local cases in the first and second waves," and "residences of local cases in the third wave," respectively. The LSBGs of the visited locations in Figure 8 are categorized similarly, with "IV 1&2," "LV 1&2," and "LV 3" representing "buildings/venues visited by imported cases in the first and second waves," "buildings/venues visited by local cases in the first and second waves," and "buildings/venues visited by local cases in the third wave," respectively. There is no "IR 3" or "IV 3" group because there were few imported cases in the third wave of COVID-19 in Hong Kong. In the figures, the category of clusters with red color and (*) means that for the category, there is a significant difference in the

feature between the clustered LSBGs and non-clustered LSBGs, which indicates that the feature is significantly associated with a higher COVID-19 risk of the locations in this category. The category of clusters with blue color means that the feature does not contribute to the clustering of LSBGs in this category.

Figure 7 shows the distribution of the 13 features of clustered LSBGs and non-clustered LSBGs for the residences of the confirmed cases. It shows that the differences in most of the features between the clustered LSBGs and non-clustered LSBGs are significant. In Figure 7a, the median household income of the clustered LSBGs is significantly higher than that of the non-clustered LSBGs of imported cases and local cases in the first and second waves (IR 1&2 and LR 1&2). However, the median household income of the clustered LSBGs is significantly lower than that of the non-clustered LSBGs in the third wave (LR 3). The result corroborates the findings in Section 3.1 that most of the clusters of COVID-19 in the first and second waves are wealthy neighborhoods, while many of the clusters in the third wave are low-income neighborhoods. The population density in Figure 7b shows a similar pattern as the median household income, that is, population density in the residences of the clustered LSBGs in the first and second waves is lower than that of the non-clustered LSBGs, while population density of the high-risk areas in the third wave is higher than that of the non-clustered LSBGs. It indicates that the confirmed cases in the first and second waves are of higher socioeconomic status and tend to live in areas with lower population density than those in the third wave.

In terms of the built-environment features, clustered LSBGs in the first and second waves are also different from those in the third wave. As Figure 7c–m show, the clustered LSBGs of the residences of imported cases in the first and second waves (IR 1&2) are of lower building height, with more sky view, lower nodal accessibility, more green space, higher private residential land density, lower public residential land density, and lower transport land density. It characterizes the places resided in by imported cases in the first and second waves, that is, private residential areas with lower building height, lower accessibility and public transport services, more green space, and better sky view. These areas are typical wealthy areas in Hong Kong, such as the affluent neighborhoods on Hong Kong Island. This is probably because most of the imported cases in the first and second waves of COVID-19 were people working or studying overseas, who may have higher socioeconomic status than other population groups. The clustered LSBGs of the residences of local cases in the first and second waves are of higher building density, higher building height, less sky view, fewer green spaces, higher private residential land density, lower private residential land density, higher commercial land density, and higher transport land density. It shows that the LSBGS of the residences of local cases in the first and second waves are likely to be dense and high-rise areas of highly mixed residential, commercial, and transport land use.

The clustered LSBGs of the residences of local cases in the third wave are of higher building density, less sky view, higher nodal accessibility, fewer green spaces, lower open spaces and recreational land density, higher commercial and transport land density. It can be observed that the clustered LSBGs of LR 1&2 and LR 3 have higher building density, less sky view and fewer green spaces, higher commercial and transport land density. However, compared with the clustered LSBGs of LR 1&2, clustered LSBGs of LR 3 have higher accessibility but lower open spaces and recreational land density. In addition, neither the feature of private residential land density nor public residential land density is significant for the clustered LSBGs of LR 3, which is probably because the clustered LSBGs of LR 3 are a mix of public and private residential neighborhoods and other residences such as nursing homes. Since the public residences are provided by the government for low-income households, the higher public residential density in clustered LSBGs of LR 3 than that of LR 1&2 clusters also indicates that the neighborhoods in the third wave have lower socioeconomic status than those of the first and second waves.

Figure 8 shows the characteristics of the venues/buildings visited by imported cases and local cases in the first and second waves (IV 1&2 and LV 1&2) and the third wave (IV 3). It shows that the features of the LSBGs visited by confirmed cases are very different from those of the residences in Figure 7. In Figure 8a, the clustered LSBGs of IV 1&2 and LV 1&2 do not have median household income as a significant feature, compared with their corresponding non-clustered LSBGs. However, the median household income of clustered LSBGs of LV 3 is significantly lower than that of non-clustered LSBGs. In Figure 8b, the clustered LSBGs of all of IV 1&2, LV 1&2, and

LV 3 have higher population density than those of the non-clustered LSBGs. In addition to population density, the clustered LSBGs of IV 1&2, LV 1&2, and LV 3 have many similar features, including higher building density, less sky view, higher nodal accessibility, fewer green spaces, higher private residential land density, higher commercial land density, and higher transport land density. It indicates that these characteristics are likely to attract people to visit. The clustered LSBGs of LV 1&2 and LV 3 also have a lower land use mix than that of the non-clustered LSBGs, which indicates that certain types of land use (e.g., commercial and transport) are more likely to attract local confirmed cases to visit than the land use mix. Other significant features that attract confirmed cases include lower public residential land density in the clustered LSBGs of IV 1&2 and LV 1&2, and lower open spaces and recreational land density in the clustered LSBGs of IV 1&2. Figure 8 shows that the venues and places visited by the confirmed cases in the first and second waves and the third wave share more similar characteristics than those of the residences of the confirmed cases. More resources and intervention measures should be targeted at areas with such features in response to the transmission of COVID-19.

4 | DISCUSSION AND CONCLUSIONS

This study explores the space-time patterns of high-risk areas during the first and second waves and the third wave of COVID-19 in Hong Kong and the associated demographic and built-environment characteristics. Detailed knowledge and insights are generated by categorizing case-related locations in different waves into four different types: residences of local cases (LR), residences of imported cases (IR), buildings/venues visited by local cases (LV), and buildings/venues visited by imported cases (IV). Generally, COVID-19 in the third wave has a wider transmission range and longer spreading period than the first and second waves. The first COVID-19 case in Hong Kong was imported from Mainland China on January 23, 2020, which caused the first wave of COVID-19. However, the spread was quickly controlled and the number of confirmed cases remained low. As the COVID-19 pandemic overseas deteriorated in early March, many Hong Kong residents working or studying overseas returned to Hong Kong, which led to an increasing number of imported cases and local cases. The clusters of local cases in the first and second waves emerged during late March and early April, while the clusters of imported cases in the first and second waves emerged during early March and early April, which confirmed that the outbreaks of local cases lagged behind those of imported cases.

The government thereafter took a series of measures to prevent the further spread of COVID-19 from imported cases. From April 8, all inbound travelers who arrived at the Hong Kong International Airport were required to test for COVID-19. Those who tested positive were sent to hospitals immediately for treatment. In comparison with the first and second waves, the confirmed cases in the third wave were mainly local cases. The clusters of local cases in the third wave occurred mainly between early July and mid-August, and were concentrated in Kowloon and the New Territories. Most of the control measures for the imported cases were still enforced during the third wave, including testing for COVID-19 upon arrival and quarantine. However, lapses in the control measures were questioned by the public, especially the exemption of several groups of people—including sailors, airline crew members, and executives of companies—upon entering Hong Kong, which was described as a "loophole" of the pandemic control system. As found in Section 3.1, a cluster of venues visited by imported cases at the beginning of the third wave (between July 8 and 13) included a cargo plane pilot exempted from testing and quarantine requirements. Thus, it is likely that the third wave of COVID-19 in Hong Kong was partly caused by the exemption of these groups of people.

The findings of this study also show that in the first and second waves of COVID-19, local cases are more likely to reside in areas with high-rise and dense buildings, as well as highly mixed residential, commercial, and transport land uses. The places resided in by the imported cases in the first and second waves are more likely to be private residential areas with lower building height, lower accessibility, and less public transport service, more green spaces and better sky view. The residences of both the local cases and imported cases in the first and second waves are areas with higher income and lower population density. In contrast, the residences of the local

cases in the third wave are associated with lower income, higher population density and higher building density, less sky view, fewer green spaces, and lower open spaces and recreational land density, but higher commercial and transport land use density and higher accessibility. Those areas contain both private residences and public residences with lower income, such as Sham Shui Po and Tze Wan Shan. In the third wave, outbreaks occurred in different local neighborhoods, schools, and nursing homes. Many vulnerable groups were infected including the elderly, low-income workers, and taxi drivers.

Different from the residences of the confirmed cases in the first and second waves and the third wave, venues and buildings visited by the confirmed cases in the first and second waves and the third wave have many characteristics in common. Generally, these locations are areas with higher population density, dense and high-rise buildings, less sky view and fewer green spaces, higher private residential, commercial, and transport land use density. Venues that were frequently visited include bars and restaurants, shopping malls and markets in residential neighborhoods, which were also the workplaces of some local cases who were infected at these places. The findings in this study indicate that resources and prevention measures should be focused on and implemented in these venues or venues with such characteristics, in order to decrease the transmission risk of COVID-19.

This study finds that the confirmed cases in the first and second waves and the third wave are likely to be different groups of the population, with those in the first and second waves having higher income and those in the third wave having lower income. With imported cases as the sources of COVID-19 transmission in both waves, the findings of this study are informative. In the first and second waves, although there were a large number of imported cases who went outdoors and conducted activities at places before the 14-day quarantine policy was issued or by violating the 14-day quarantine rule, the imported cases did not cause large-scale outbreaks of local cases. On the one hand, there were fewer imported cases going out during the first and second waves than those exempted in the third wave. Most of the places visited by the confirmed cases in the first and second waves could be tracked, which helped the control efforts. However, there were around 200,000 people exempted from quarantine in the third wave. Some of those (such as airline crew members and sailors) visited certain places and then left Hong Kong. Thus, the places visited by these people could not be tracked, which may increase the risks of COVID-19 transmission.

On the other hand, during the initial period of COVID-19 (i.e., from January to April 2020 in the first and second waves), Hong Kong residents were very nervous about the pandemic and proactively cooperated with the government's social distancing and other control measures. However, by the end of June, many people felt fatigued after months of social distancing. Considering the easing situation of the pandemic and the need for economic recovery, the government allowed public gatherings of up to 50 people. Residents in Hong Kong also began meeting with friends and family and conducting social gatherings, which further increased the transmission risk of COVID-19. It is also reported in Rypdal, Bianchi, and Rypdal (2020) that “intervention fatigue” is the major cause of the second waves of COVID-19 in European countries. By comparing the first and second waves and the third wave of COVID-19 in Hong Kong, we found that when COVID-19 transmission risk is higher, local communities with lower income and higher population density have a higher risk of pandemic outbreaks, and the most vulnerable groups include entry-level workers, service workers, the elderly, and people with high-risk occupations like taxi drivers.

The findings in this study have several policy implications. First, it identified the high-risk areas of COVID-19 in the first and second waves and the third wave, and these areas respectively represent the imported-case-dominated and local-case-dominated COVID-19 landscapes of Hong Kong. The findings for different waves can serve as references for subsequent pandemic prevention and control. Second, the built-environment features associated with higher transmission risks can inform policymakers to implement stricter mitigation measures such as social distancing, banning activities in places with such features, and advising people to avoid conducting high-risk activities and visiting such places. As our knowledge about the impact of the built and social environments on the spread of COVID-19 is highly limited to date, this study also contributes to the literature by analyzing the space-time patterns of the areas with higher COVID-19 transmission risk and the associated demographic and built-environment characteristics in a compact and socioeconomically segregated city like Hong Kong. In this study, the contact tracing information of each confirmed case was obtained, making it possible to characterize the

patterns of the residences of, and places visited by, the confirmed cases. This study highlights the significance of contact tracing information and high-resolution demographic and built-environment datasets in describing, explaining, and predicting the high-risk areas and population groups during a pandemic like COVID-19 using space-time clustering techniques.

In this study we avoided detecting LSBGs divided by the harbor as being a cluster, by adjusting the spatial and temporal windows in the space-time scan statistic. However, we did not consider elements of the transportation system as physical barriers that prevent people's interactions and the spread of COVID-19, which is a limitation of the study.

ACKNOWLEDGEMENTS

The authors thank the anonymous reviewers for their helpful comments. Zihan Kan was supported by an RGC Postdoctoral Fellowship from the Research Grants Council of Hong Kong (PDFS2021-4S08). Mei-Po Kwan was supported by grants from the Hong Kong Research Grants Council (General Research Fund Grant no. 14605920; Collaborative Research Fund Grant no. C4023-20GF) and a grant from the Research Committee on Research Sustainability of Major Research Grants Council Funding Schemes of the Chinese University of Hong Kong. Man Sing Wong thanks the funding support of a grant from the Hong Kong Research Grants Council (General Research Fund Grant no. 15602619) and the Research Institute for Sustainable Urban Development (Grant no. 1-BBWD) of the Hong Kong Polytechnic University. Dong Liu was supported by a Marion G. Russell Graduate Fellowship from the University of Illinois at Urbana-Champaign.

DATA AVAILABILITY STATEMENT

All the data used in the study are publicly available via various government websites in Hong Kong.

ORCID

Zihan Kan https://orcid.org/0000-0002-6364-0537
Mei-Po Kwan https://orcid.org/0000-0001-8602-9258
Jianwei Huang https://orcid.org/0000-0002-2230-3446
Man Sing Wong https://orcid.org/0000-0002-6439-6775
Dong Liu https://orcid.org/0000-0001-9090-5732

REFERENCES

Desjardins, M., Hohl, A., & Delmelle, E. (2020). Rapid surveillance of COVID-19 in the United States using a prospective space-time scan statistic: Detecting and evaluating emerging clusters. *Applied Geography*, *118*, 102202. https://doi.org/10.1016/j.apgeog.2020.102202

Dietz, L., Horve, P. F., Coil, D. A., Fretz, M., Eisen, J. A., & Van Den Wymelenberg, K. (2020). 2019 novel coronavirus (COVID-19) pandemic: Built environment considerations to reduce transmission. *Msystems*, *5*(2), e00245-20. https://doi.org/10.1128/mSystems.00245-20

Frank, L., Engelke, P., & Schmid, T. (2003). *Health and community design: The impact of the built environment on physical activity*. Washington, DC: Island Press.

Gao, S., Rao, J., Kang, Y., Liang, Y., & Kruse, J. (2020). Mapping county-level mobility pattern changes in the United States in response to COVID-19. *SIGSPATIAL Special*, *12*(1), 16–26. https://doi.org/10.1145/3404820.3404824

Garfinkel-Castro, A., Kim, K., Hamidi, S., & Ewing, R. (2017). Obesity and the built environment at different urban scales: Examining the literature. *Nutrition Reviews*, *75*(Suppl. 1), 51–61. https://doi.org/10.1093/nutrit/nuw037

Gori, S., Nigro, M., & Petrelli, M. (2012). The impact of land use characteristics for sustainable mobility: The case study of Rome. *European Transport Research Review*, *4*(3), 153–166. https://doi.org/10.1007/s12544-012-0077-6

Hohl, A., Delmelle, E. M., Desjardins, M. R., & Lan, Y. (2020). Daily surveillance of COVID-19 using the prospective space-time scan statistic in the United States. *Spatial and Spatiotemporal Epidemiology*, *34*, 100354. https://doi.org/10.1016/j.sste.2020.100354

Huang, J., Kwan, M.-P., Kan, Z., Wong, M. S., Kwok, C. Y. T., & Yu, X. (2020). Investigating the relationship between the built environment and relative risk of COVID-19 in Hong Kong. *ISPRS International Journal of Geo-Information*, *9*(11), 624. https://doi.org/10.3390/ijgi9110624

Kan, Z., Kwan, M.-P., Wong, M. S., Huang, J., & Liu, D. (2021). Identifying the space-time patterns of COVID-19 risk and their associations with different built environment features in Hong Kong. *Science of the Total Environment*, *772*, 145379. https://doi.org/10.1016/j.scitotenv.2021.145379

Kirby, R. S., Delmelle, E., & Eberth, J. M. (2017). Advances in spatial epidemiology and geographic information systems. *Annals of Epidemiology*, *27*(1), 1–9. https://doi.org/10.1016/j.annepidem.2016.12.001

Koohsari, M. J., Badland, H., & Giles-Corti, B. (2013). (Re) Designing the built environment to support physical activity: Bringing public health back into urban design and planning. *Cities*, *35*, 294–298. https://doi.org/10.1016/j.cities.2013.07.001

Kraemer, M. U. G., Yang, C.-H., Gutierrez, B., Wu, C.-H., Klein, B., Pigott, D. M., … Scarpino, S. V. (2020). The effect of human mobility and control measures on the COVID-19 epidemic in China. *Science*, *368*(6490), 493–497. https://doi.org/10.1126/science.abb4218

Kulldorff, M. (2001). Prospective time periodic geographical disease surveillance using a scan statistic. *Journal of the Royal Statistical Society: Series A (Statistics in Society)*, *164*(1), 61–72. https://doi.org/10.1111/1467-985X.00186

Kulldorff, M. (2018). *SaTScan*™ *User Guide for version 9.6*. Retrieved from http://www.satscan.org/

Kwok, C. Y. T., Wong, M. S., Chan, K. L., Kwan, M.-P., Nichol, J. E., Liu, C. H., … Kan, Z. (2021). Spatial analysis of the impact of urban geometry and socio-demographic characteristics on COVID-19: A study in Hong Kong. *Science of the Total Environment*, *764*, 144455. https://doi.org/10.1016/j.scitotenv.2020.144455

Markevych, I., Schoierer, J., Hartig, T., Chudnovsky, A., Hystad, P., Dzhambov, A. M., … Fuertes, E. (2017). Exploring pathways linking greenspace to health: Theoretical and methodological guidance. *Environmental Research*, *158*, 301–317. https://doi.org/10.1016/j.envres.2017.06.028

Mollalo, A., Vahedi, B., & Rivera, K. M. (2020). GIS-based spatial modeling of COVID-19 incidence rate in the continental United States. *Science of The Total Environment*, *728*, 138884. https://doi.org/10.1016/j.scitotenv.2020.138884

Mulatti, P., Mazzucato, M., Montarsi, F., Ciocchetta, S., Capelli, G., Bonfanti, L., & Marangon, S. (2015). Retrospective space-time analysis methods to support West Nile virus surveillance activities. *Epidemiology & Infection*, *143*(1), 202–213. https://doi.org/10.1017/S0950268814000442

Prates, M. O., Kulldorff, M., & Assunção, R. M. (2014). Relative risk estimates from spatial and space-time scan statistics: Are they biased? *Statistics in Medicine*, *33*(15), 2634–2644. https://doi.org/10.1002/sim.6143

Raifman, M. A., & Raifman, J. R. (2020). Disparities in the population at risk of severe illness from Covid-19 by race/ethnicity and income. *American Journal of Preventive Medicine*, *59*(1), 137–139. https://doi.org/10.1016/j.amepre.2020.04.003

Robertson, C., & Nelson, T. A. (2010). Review of software for space-time disease surveillance. *International Journal of Health Geographics*, *9*(1), 16. https://doi.org/10.1186/1476-072X-9-16

Rypdal, K., Bianchi, F. M., & Rypdal, M. (2020). Intervention fatigue is the primary cause of strong secondary waves in the COVID-19 pandemic. *International Journal of Environmental Research and Public Health*, *17*(24), 9592. https://doi.org/10.3390/ijerph17249592

Soliman, A., Soltani, K., Yin, J., Padmanabhan, A., & Wang, S. (2017). Social sensing of urban land use based on analysis of Twitter users' mobility patterns. *PLoS ONE*, *12*(7), e0181657. https://doi.org/10.1371/journal.pone.0181657

Takahashi, K., Kulldorff, M., Tango, T., & Yih, K. (2008). A flexibly shaped space-time scan statistic for disease outbreak detection and monitoring. *International Journal of Health Geographics*, *7*(1), 14. https://doi.org/10.1186/1476-072X-7-14

Tang, X., Geater, A., McNeil, E., Deng, Q., Dong, A., & Zhong, G. (2017). Spatial, temporal and spatio-temporal clusters of measles incidence at the county level in Guangxi, China during 2004–2014: Flexibly shaped scan statistics. *BMC Infectious Diseases*, *17*(1), 243. https://doi.org/10.1186/s12879-017-2357-1

Tiwari, C., & Rushton, G. (2010). A spatial analysis system for integrating data, methods and models on environmental risks and health outcomes. *Transactions in GIS*, *14*, 177–195. https://doi.org/10.1111/j.1467-9671.2010.01220.x

Wang, P., Goggins, W. B., Zhang, X., Ren, C., & Lau, K.- K.-L. (2020). Association of urban built environment and socioeconomic factors with suicide mortality in high-density cities: A case study of Hong Kong. *Science of The Total Environment*, *739*, 139877. https://doi.org/10.1016/j.scitotenv.2020.139877

Whiteman, A., Desjardins, M. R., Eskildsen, G. A., & Loaiza, J. R. (2019). Detecting space-time clusters of dengue fever in Panama after adjusting for vector surveillance data. *PLoS Neglected Tropical Diseases*, *13*(9), e0007266. https://doi.org/10.1371/journal.pntd.0007266

Yang, J., Wong, M. S., Menenti, M., & Nichol, J. (2015). Modeling the effective emissivity of the urban canopy using sky view factor. *ISPRS Journal of Photogrammetry and Remote Sensing*, *105*, 211–219. https://doi.org/10.1016/j.isprsjprs.2015.04.006

How to cite this article: Kan, Z., Kwan, M.-P., Huang, J., Sing Wong, M., & Liu, D. (2021). Comparing the space-time patterns of high-risk areas in different waves of COVID-19 in Hong Kong. *Transactions in GIS*, 00, 1–20. https://doi.org/10.1111/tgis.12800